

Measurement of Time-Dependent Drive Flux on the Capsule for Indirectly Driven Inertial Confinement Fusion Experiments


Xufei Xie¹,[✉] Lifei Hou,¹ Hongbo Cai^{1,2,3,*}, Changshu Wu,² Xiaoshi Peng,¹ Xiaoxi Duan,¹ Shenyue Liu,¹ Dong Yang,¹ Sanwei Li,¹ Zhichao Li,¹ Qi Li,¹ Yonggang Liu,¹ Huabin Du,¹ Kuan Ren,¹ Fengjun Ge,² Weiming Yang,¹ Liang Guo,¹ Wanli Shang,¹ Xingsen Che,¹ Longfei Jing,¹ Yulong Li,¹ Huiyue Wei,¹ Yimeng Yang,¹ Ao Sun,¹ Ruizhen Yu,¹ Yunbao Huang,⁴ Xiaohua Jiang,¹ Tao Xu,¹ Xiaohan He,¹ Chaoguang Li,¹ Yingjie Li,¹ Feng Wang,¹ Haien He,¹ Jiamin Yang,^{1,†} Kai Du,¹ Shaoen Jiang,¹ Baohan Zhang,¹ and Yongkun Ding^{2,3}

¹Laser fusion Research Center, Chinese Academy of Engineering Physics, Mianyang 621900, China

²Institute of Applied Physics and Computational Mathematics, Beijing, 100088, China

³Center for Applied Physics and Technology, HEDPS, and College of Engineering, Peking University, Beijing 100871, China

⁴Mechatronics School of Guangdong University of Technology, Guangzhou 510080, China

 (Received 8 September 2020; revised 6 April 2021; accepted 7 April 2021; published 15 February 2022)

A new method for measuring the time-dependent drive flux at the hohlraum center is proposed as a better alternative to conventional wall-based techniques. The drive flux here is obtained by simultaneous measurement of the reemitted flux and shock velocity from a three-layered “cakelike” sample. With these two independent observables, the influence induced by the uncertainty of the material parameters of the sample can be effectively decreased. The influence from the closure of the laser entrance hole, which was the main challenge in conventional wall-based techniques, was avoided through localized reemitted flux measurement, facilitating drive flux measurement throughout the entire time history. These studies pave a new way for probing the time-dependent drive flux, for both cylindrical hohlraums and novel hohlraums with six laser entrance holes.

DOI: [10.1103/PhysRevLett.128.075001](https://doi.org/10.1103/PhysRevLett.128.075001)

Hohlraums are often adopted for the conversion of high-power laser energy to x-ray radiations, and hohlraum radiation source has broad applications in high-energy-density investigations, such as indirect drive inertial confinement fusion [1,2], opacity parameters [3], radiation transport [4], astrophysics [5], etc. In recent years, great progress has been made using optimized hohlraums, such as near-vacuum hohlraum [6] and depleted uranium hohlraum [7–10], where both the intensity and uniformity of the drive flux on the capsule are improved. However, the time-dependent drive flux on the capsule throughout the entire time history remains unmeasured in integrated implosion experiments, which is still regarded as the largest source of uncertainty in numerical simulations [11]. Conventionally, the drive flux on the capsule was determined by comparing the time-dependent radiation flux from the hohlraum wall via laser entrance holes (LEHs) [12–14]. However, the wall-based techniques proved to be affected by the LEH closure, as revealed in the ViewFactor experiment [15]. In integrated implosion experiments approaching burning plasma at the National Ignition Facility, models benchmarked with wall-based techniques were found to overpredict the drive flux by up to ~15%, which was known as “drive deficit” [16].

With the underlying physical reason for the drive deficit remaining ambiguous, the x-ray drive on the capsule was

then treated as an adjustable parameter to be modified as necessary to reproduce the implosion observables in capsule-only simulations [17]. The ultimately “tuned” drive flux, which was consistent with the shock velocity and shock merger time [18], as well as the implosion trajectory and hot spot x-ray self-emission shape data, was regarded as the “effective radiation drive.” Although it should not be interpreted as an accurate representation of the drive flux on the capsule, it can best reproduce the implosion characteristics measured in experiments. However, given the importance of the drive flux, it is important and worthwhile to develop better diagnostic of the time-dependent radiation drive throughout the entire time history, which is essential for the improvement of the physical model and the predictive capability of the simulations.

In this Letter, we present a novel method to assess the time-dependent drive flux by simultaneously measuring the shock velocity and the localized reemitted flux from the same sample at the hohlraum center. Here, the shock velocity in well-characterized opaque samples can provide direct evidence of the peak drive flux [19,20]. Meanwhile, the time-dependent reemitted flux from the same sample, which is obtained via a localized radiation flux measurement technique [21,22], serves as another crucial constraint throughout the entire time history. Note that the conventional wall-based techniques were easily affected by the

ambiguous assessment of the LEH closure; however, in our work, the influence from the LEH closure can be avoided. The time-dependent drive flux is then determined with the support of radiation hydrodynamic (RH) simulations. Notably, these two independent observables can also provide a validation cross-check for the opacity and equation-of-state parameters of the sample, as both the observables can be reproduced only with a unique and correct set of parameters. In this context, with the two observables, the influence induced by the uncertainty of the sample parameters can be effectively decreased in comparison with only one observable. Moreover, for the technique presented here, a standard sample with well-known opacity and equation-of-state parameters is not essential, as other samples can also be employed.

The experiment described herein demonstrates, for the first time, measurement of the time-dependent drive flux by simultaneously measuring the shock velocity and the reemitted flux. Schematic illustration of the experiment with Shenguang hohlraums [23] is presented in Fig. 1. A cylindrical gold (Au) hohlraum with a diameter of 2.4 mm and a length of 4.3 mm was adopted. The three-layered sample was placed at the hohlraum center with a keyhole, which is a gold reentrant conical tube entering through the hohlraum wall providing optical access to the propagating shocks. Generally, a sample with a continuously varying thickness can provide a shock velocity trace for the drive source scaling [19]. However, to determine the sample thickness more precisely, a sample with a discretely varying thickness was employed. Each layer was cylindrical and made of aluminum, composed of a “cakelike” sample. To prevent the preheating induced by the M -band flux, a base composed of Au was added at the bottom of the three-layered sample, while another aluminum base was added as the ablation layer. The diameters of the aluminum base and Au base were approximately $1200\ \mu\text{m}$, with thicknesses of 14.4 and $4.4\ \mu\text{m}$, respectively. The diameters of the three

aluminum layers were 1200 , 700 , and $400\ \mu\text{m}$, with thicknesses of 50.1 , 19.9 , and $19.7\ \mu\text{m}$, respectively. The thickness was chosen so that the change of the shock velocity in layer 2 and layer 3 was relatively slow.

A diagnostic hole was located at the waist of the hohlraum and in front of the sample, with a diameter of $1000\ \mu\text{m}$, and it was used for the measurement of the reemitted flux. To suppress the movement of the Au bubble, the hohlraum was filled with neopentane (C_5H_{12}) gas at a density of approximately $0.9\ \text{mg/cc}$. Thirty-two laser beams were arranged to irradiate the inside of the hohlraum in two rings, with an incident angle of 49.5° or 55° relative to the hohlraum axis. A square laser pulse was used, the length of the flat-topped pulse was $1\ \text{ns}$, with a wavelength of $0.351\ \mu\text{m}$, and the total laser energy was approximately $26.7\ \text{kJ}$.

The reemitted flux from the sample was obtained by a space-resolving flux detector (SRFD) [24], which directed toward the planar surface of the sample through the diagnostic hole. The temporal resolution of the SRFD system is approximately $120\ \text{ps}$, while the x-ray energy range covered by the system is $0.1\text{--}4\ \text{keV}$. Here, the diameter of the view field for the SRFD system at the hohlraum center was only approximately $400\ \mu\text{m}$, which was small enough to avoid the influence of the closure of the diagnostic hole (with a diameter of $1000\ \mu\text{m}$) on the localized reemitted flux measurement. Furthermore, the influence of radiation flux from the filling plasma along the line of sight was negligible. Meanwhile, the shock wave image was measured from the opposite side of the sample with a streaked optical pyrometer (SOP). For comparison, three flat-response x-ray diode (FXRD) detectors [25] were employed to measure the radiation flux escaping from the LEHs, which were located at up 16° , up 42° , and down 42° relative to the hohlraum axis, respectively, and the view fields are presented in Fig. 1(c).

The results measured by the SRFD system are presented in Fig. 2. The location of the view field can be determined using the image obtained by the CCD camera in the SRFD system, as illustrated in Fig. 2(b). One can see that the offset between the center of the view field and the sample is approximately $22.4\ \mu\text{m}$. Given that the diameter of the sample is approximately $1200\ \mu\text{m}$, the offset is small enough to be neglected. Furthermore, RH simulations revealed that the difference in radiation flux was less than 0.5% due to this offset. The time-dependent radiation temperature (T_r), which represents the radiation flux measured by the SRFD system, is depicted in Fig. 2(d). This is the first time that the localized reemitted flux from the sample at the hohlraum center is obtained. For simplicity, the radiation flux is represented by the corresponding radiation temperature in the following. The radiation flux rose quickly during the first $1.0\ \text{ns}$ when the laser beams were turned on, and the increase is attributed to the reemitted flux from the sample placed at the hohlraum

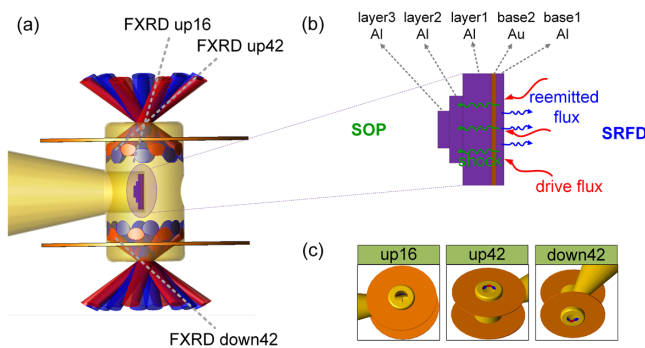


FIG. 1. (a) Sketch of the experimental configuration for simultaneous measurement of the shock velocity and reemitted flux from the same sample at the hohlraum center. (b) The SOP and SRFD systems are located at opposite sides of the sample, with a relative angle of 180° . (c) View fields of the three FXRD detectors.

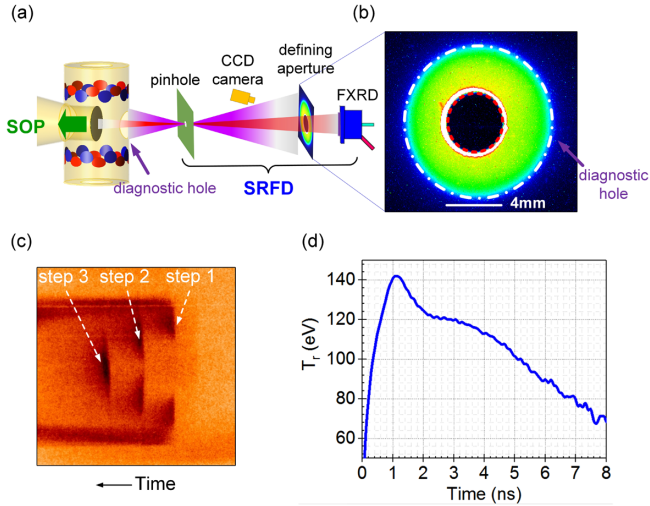


FIG. 2. (a) Schematic of the SRFD system. (b) Location of the view field for the SRFD system, where the white dash-dotted circle indicates the contour corresponding to the diagnostic hole, and the red dashed circle (with a diameter of 4 mm) indicates the contour corresponding to the view field (with a diameter of $400 \mu\text{m}$). (c) Shock wave image from the sample obtained by the SOP system. (d) The localized radiation flux measured by the SRFD system.

center. The flux dropped quickly after the lasers were turned off at 1.0 ns. However, the flux shows an abnormal hump at 3–5 ns. This hump is associated with the emission from the colliding high- Z blowoff plasma from the hohlraum wall at the hohlraum center. Its typical characteristic is that it persists for a long time and fades away slowly.

The shock wave image obtained by the SOP system is illustrated in Fig. 2(c), in which three steps generated by the shock wave can be clearly seen. One can see that these shock steps are symmetric, thereby indicating that the drive flux at the hohlraum center was symmetric with respect to the sample axis. The shock velocity within layer 2 was approximately $30.8 \pm 0.9 \text{ km/s}$, and within layer 3 it was approximately $28.5 \pm 0.8 \text{ km/s}$. After penetrating the Au base, the shock velocity decreased rapidly during the transmission within the aluminum layers, and the mean speed decreased by 2.3 km/s between layer 2 and layer 3.

RH simulations performed with the LARED-integration code [26,27] provide an overview of the plasma conditions inside the hohlraum. To reproduce the measured reemitted flux and shock velocity simultaneously, detailed adjustments were made to the flux limiter in the flux-limited model, while the opacity multiplier and equation-of-state parameters were carefully selected. Notably, with conventional wall-based techniques, RH simulation results were adjusted to be consistent with the measured fluxes from the hohlraum wall, and then the drive flux on the capsule was deduced. However, in our work, the first priority for the simulation adjustments was that the measured shock velocity and reemitted flux need to be satisfied

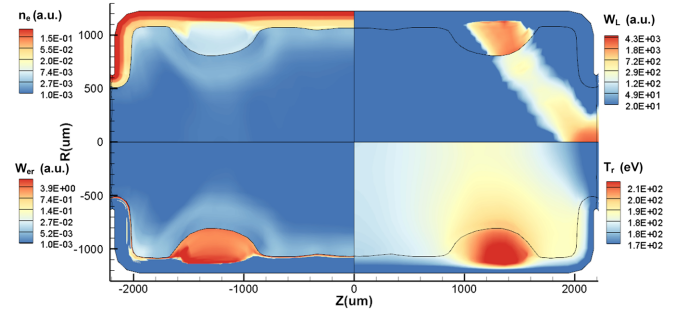


FIG. 3. Simulated spatial distributions of the normalized electron density n_e , the deposited laser energy W_L , the x-ray emissivity W_{er} , and the radiation temperature T_r inside the hohlraum at $t = 1.0 \text{ ns}$.

simultaneously. We then compared the difference between the measured and simulated fluxes from the hohlraum wall. With all of the observations satisfied with the simulations, the drive flux at the hohlraum center was determined.

Figure 3 illustrates the spatial distributions of the normalized electron density n_e , the deposited laser energy W_L , the x-ray emissivity W_{er} , and the radiation temperature T_r inside the hohlraum at $t = 1.0 \text{ ns}$. Here, $n_e = N_e/N_c$, and N_e is the electron density while N_c is the critical electron density for the laser with a wavelength of $0.351 \mu\text{m}$. The laser energy is mainly deposited at the critical surface; after the laser is shut down, the electron temperature begins to decrease together with the x-ray emissivity (with an energy range of 0.1–4 keV). At 1.0 ns, the gold bubble moves toward the hohlraum axis with an approximate velocity of $400 \mu\text{m/ns}$, but it does not reach the hohlraum axis. This indicates that the reemitted flux from the sample surface is the dominant component in the signal measured by the SRFD system during the laser injection.

The time-dependent drive flux on the sample was obtained using LARED-integration simulations, as illustrated in Fig. 4(a). Although the sample was not accounted for in the simulations, the influence of the reentrant conical tube and diagnostic hole on the drive flux was evaluated and corrected in detail, and it was revealed that the drive flux decreased by approximately 5 eV in peak value [28]. Then, one-dimensional RH simulations using RDMG [33] were performed to calculate the resulting reemitted flux and shock velocity. It was found that the simulated reemitted flux was consistent with the measured flux, as presented in Fig. 4(a). The slight discrepancy at the beginning is mainly due to the backscatter. Notably, the drive flux F_d can be related to the reemitted flux F_{re} through the albedo of the sample (α_{sample}):

$$F_{re} = \alpha_{\text{sample}} F_d. \quad (1)$$

Given $F_{re} = \sigma T_{re}^4$ and $F_d = \sigma T_d^4$, where σ is the Stefan-Boltzmann constant, the time evolution of α_{sample} can be obtained by

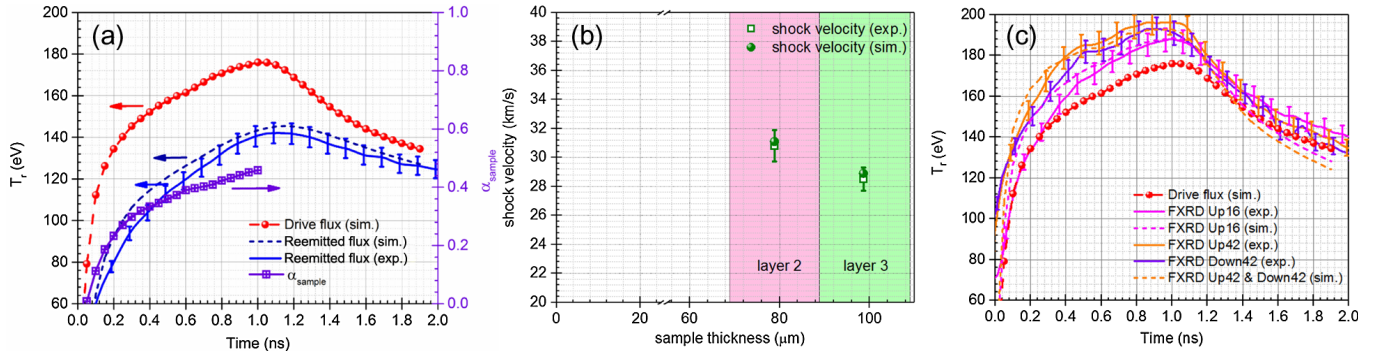


FIG. 4. (a) Comparison of the measured and calculated radiation flux from the sample together with the simulated drive flux at the hohlraum center. The time-varying albedo of the sample (α_{sample}) is presented as the purple solid line. (b) Comparison of the measured and calculated shock velocities within layer 2 and layer 3. (c) Simulated drive flux at the hohlraum center together with measured and simulated fluxes from the FXRD detectors are plotted for comparison.

$$\alpha_{\text{sample}}(t) = \left(\frac{T_{\text{re}}(t)}{T_d(t)} \right)^4, \quad (2)$$

where $T_d(t)$ represents the temperature for the drive flux incident on the sample and $T_{\text{re}}(t)$ represents the temperature for the reemitted flux from the sample, respectively. As presented by the solid purple line in Fig. 4(a), it was found that α_{sample} increases rapidly with the laser injection, and it reached approximately 0.46 at 1.0 ns.

Note that, with only the measured reemitted flux F_{re} , the drive flux F_d can be obtained with Eq. (1). However, this method is complicated by the fact that the albedo α_{sample} is also sensitive to the drive flux F_d . One solution for this complication is forward fitting. With a preset drive flux, the albedo can be deduced and the reemitted flux can be calculated. By adjusting the preset drive flux and comparing the calculated reemitted flux with the measured data, the drive flux can be finally determined.

In our work, however, we utilized another solution, which untangles the interdependence between the drive flux and albedo with the help of shock velocity. The shock velocity is also related to the drive flux as well as the opacity and equation-of-state parameters of the sample, and it serves as another important constraint. A comparison between the simulated and measured shock velocities is illustrated in Fig. 4(b). Simulations showed that the shock velocities were approximately 31.1 and 28.9 km/s in layer 2 and layer 3, respectively. These values are in good agreement with the measured data.

With simultaneous measurement of the reemitted flux and shock velocity from the same sample, the opacity and equation-of-state parameters of the sample material could be cross-checked, and the drive flux could be exclusively determined. Here, a simplified analysis is conducted for a stationary ablation process on a planar sample. With the drive source T_d constant in time, the albedo α can be expressed as $1 - \alpha = C_1 \bar{E} / t T_d^4$, with wall loss per unit area $\bar{E} = C_2 \epsilon \times m_F$. Here, ϵ is the internal energy and m_F is the

Marshak front areal density $m_F = C_3 \sqrt{T_d^4 t / \kappa \epsilon}$, with κ as opacity [34]. C_1 , C_2 , and C_3 are constant coefficients. Therefore, the reemitted flux F_{re} can be related to the opacity as

$$F_{\text{re}} = \alpha \cdot \sigma T_d^4 = \left(1 - C_1 C_2 C_3 \sqrt{\frac{\epsilon}{\kappa t T_d^2}} \right) \cdot \sigma T_d^4. \quad (3)$$

Meanwhile, for the stationary x-ray drive ablation process, the relation between the radiation temperature T_d and the shock speed U_s can be obtained through the ablation pressure $P = D_1 (1 - \alpha) T_d^4 / U_p = D_2 \rho U_s^2$, where U_p is the ablated particle speed which is of the order of sound speed $U_p = D_3 \sqrt{Z_0 T_d / A}$, with Z_0 as the average degree of ionization, ρ as the density, and A as the mass number, and D_1 , D_2 , and D_3 are the constant coefficients. Hence, the shock speed is related with the opacity as

$$U_s = C_{\text{sh}} \rho^{-1/2} \left(\frac{\epsilon A}{\kappa t Z_0} \right)^{1/4} T_d^{3/4}, \quad (4)$$

where $C_{\text{sh}} = \sqrt{D_1 C_1 C_2 C_3 / D_2 D_3}$. With $F_{\text{re}} \sim \kappa^{-0.5}$ and $U_s \sim \kappa^{-0.25}$, only the uniquely correct opacity and drive flux can reproduce the experimental observations simultaneously. Therefore, good agreements between experiment and simulation indicate that the drive flux was accurately determined with our technique, which is a significant advantage over the forward-fitting method, which merely relies on the measured reemitted flux [28]. Meanwhile, it should also be noted that this technique can be applied for the detailed investigation of the opacity and equation-of-state parameters, which are important for reliable modeling and understanding many phenomena in high-energy-density physics.

Moreover, the radiation fluxes for the FXRD detectors were also obtained by the postprocess of the RH simulations. Comparison between the measured and simulated

radiation fluxes is illustrated in Fig. 4(c). One can see that RH simulations could also reproduce the experimental data for all three viewing angles.

In Fig. 4(c), the drive flux is compared with the radiation fluxes measured by the FXRD detectors from the hohlraum wall. One can see that the drive flux is quite distinguished from the other three, in terms of both absolute intensity and temporal behavior. The peak drive flux was found to decrease by 12.0 eV compared to the FXRD detector at up 16° and by 17.1 eV for the FXRD detector at up 42° , corresponding to 7.6% and 11.2% in relative value, respectively. Note that the experimental error was only 5–6 eV [25], indicating that this difference was not due to experimental error. The measured flux through the LEH at a specific angle was usually assumed as a representative of the capsule drive [35,36]. However, the evident difference revealed by our work indicates that better techniques are needed for the detailed evaluation of the drive flux. In order to elucidate the difference between the drive flux and measured FXRD fluxes more clearly, a set of implosion simulations were performed with RDMG with a typical implosion capsule design [28]. Quantitative analysis revealed that the maximum implosion velocity can be distinguished by approximately 40 km/s, indicating that the capsule implosion is extremely sensitive to the hohlraum drive and it is of crucial importance for the detailed evaluation of the drive flux on the capsule.

It is worth noting that this technique can be applied for probing the drive flux throughout the entire time history. One hypothesis regarding the drive deficit suggests that the rate of rise of the x-ray drive in the main pulse is slower than simulations [16]. The shock timing technique is able to probe the drive flux at the early time of the drive history, but it suffers from the “blinking” effect due to the high shock speed (high pressure) of the main pulse [37]. However, with our technique, the reemitted flux from the sample can be obtained both at the early time and in the main pulse. As for the SOP measurement, it captures only the self-emission of the sample and there is no blanking effect due to the high shock speed. In this context, this technique is promising for the detailed investigation of the underlying physical reason for the drive deficit, especially during the main pulse. Meanwhile, it is interesting to note that the localized reemitted flux measurement can also be applied in the integrated implosion experiment with a standard hohlraum and a fusion capsule, where the localized reemitted flux from the capsule can provide key information of the drive flux throughout the entire time history; moreover, it is a noninvasive measurement, as the reemitted flux from the capsule can be obtained through the LEH of the hohlraum.

Furthermore, the simultaneous measurement of the localized reemitted flux and shock velocity can also be applied for the evaluation of the drive flux in novel six-LEH hohlraums, such as octahedral spherical hohlraums [27] and three-axis cylindrical hohlraums [38], for which the

radiation fluxes escaping from different LEHs cannot be distinguished experimentally using a soft x-ray spectrometer or FXRD detector. Therefore, traditional methods cannot provide a good constraint for the RH simulation codes, and novel methods are urgently needed for the evaluation of the drive flux.

In summary, we performed a pioneering work wherein we directly probed the drive flux at the hohlraum center by simultaneously measuring the reemitted flux and shock velocity from the same sample. The obtained time-dependent drive flux could reproduce the shock velocity and the reemitted flux simultaneously. A significant decrease (7.6%–11.2%) in the peak radiation temperature of the drive flux was found as compared to the measured fluxes from the hohlraum wall. These studies pave a new way for probing the drive flux throughout the entire time history. Further investigations will be focused on application of this technique in other novel hohlraums.

The authors express their gratitude to the target fabrication team and the operation group for their hard work and close collaboration. This work is supported by the National Key R&D Program of China (No. 2017YFA040330), the National Natural Science Foundation of China (Grants No. 11975216, No. 11975215, No. 11975055, No. 11705180, No. 11875241, and No. 11905204), and Research Center of Laser Fusion Funds for Young Talents.

* cai_hongbo@iapcm.ac.cn

† yjm70018@sina.cn

- [1] J. D. Lindl, *Phys. Plasmas* **2**, 3933 (1995).
- [2] S. Atzeni and J. Meyer-ter-Vehn, *The Physics of Inertial Fusion* (Oxford Science, New York, 2004).
- [3] R. F. Heeter, S. B. Hansen, K. B. Fournier, M. E. Foord, D. H. Froula, A. J. Mackinnon, M. J. May, M. B. Schneider, and B. K. F. Young, *Phys. Rev. Lett.* **99**, 195001 (2007).
- [4] C. A. Back, J. D. Bauer, O. L. Landen, R. E. Turner, B. F. Lasinski, J. H. Hammer, M. D. Rosen, L. J. Suter, and W. H. Hsing, *Phys. Rev. Lett.* **84**, 274 (2000).
- [5] F. L. Wang, S. Fujioka, H. Nishimura, D. Kato, Y.-T. Li, G. Zhao, J. Zhang, and H. Takabe, *Phys. Plasmas* **15**, 073108 (2008).
- [6] L. F. Berzak Hopkins *et al.*, *Phys. Rev. Lett.* **114**, 175001 (2015).
- [7] O. A. Hurricane *et al.*, *Nat. Phys.* **12**, 800 (2016).
- [8] D. E. Hinkel *et al.*, *Phys. Rev. Lett.* **117**, 225002 (2016).
- [9] S. Le Pape *et al.*, *Phys. Rev. Lett.* **120**, 245003 (2018).
- [10] K. L. Baker *et al.*, *Phys. Rev. Lett.* **121**, 135001 (2018).
- [11] D. S. Clark *et al.*, *Phys. Plasmas* **26**, 050601 (2019).
- [12] P. Amendt, S. G. Glendinning, B. A. Hammel, O. Landen, and L. J. Suter, *Phys. Rev. Lett.* **77**, 3815 (1996).
- [13] S. H. Glenzer *et al.*, *Phys. Rev. Lett.* **80**, 2845 (1998).
- [14] J. L. Kline *et al.*, *Phys. Rev. Lett.* **106**, 085003 (2011).
- [15] S. A. MacLaren *et al.*, *Phys. Rev. Lett.* **112**, 105003 (2014).
- [16] Lawrence Livermore National Laboratory, Laser Indirect Drive input to NNSA 2020 Report No. LLNL-TR-810573, 2020.

- [17] D. S. Clark *et al.*, *Phys. Plasmas* **20**, 056318 (2013).
- [18] H. F. Robey *et al.*, *Phys. Rev. Lett.* **108**, 215004 (2012).
- [19] R. L. Kauffman *et al.*, *Phys. Rev. Lett.* **73**, 2320 (1994).
- [20] Y. S. Li *et al.*, *Phys. Plasmas* **17**, 042704 (2010).
- [21] K. Ren *et al.*, *Opt. Express* **23**, A1072 (2015).
- [22] X. F. Xie *et al.*, *J. Instrum.* **12**, P08021 (2017).
- [23] W. G. Zheng *et al.*, *Matter Radiat. Extremes* **2**, 243 (2017).
- [24] X. F. Xie *et al.*, *Rev. Sci. Instrum.* **89**, 063502 (2018).
- [25] Z. C. Li *et al.*, *Rev. Sci. Instrum.* **81**, 073504 (2010).
- [26] W. Pei *et al.*, *Commun. Comput. Phys.* **2**, 255 (2007), http://www.global-sci.com/intro/article_detail/cicp/7905.html.
- [27] W. Y. Huo *et al.*, *Phys. Rev. Lett.* **120**, 165001 (2018).
- [28] See Supplemental Material at <http://link.aps.org/supplemental/10.1103/PhysRevLett.128.075001> for the detailed analysis for the influence of the reentrant conical tube and diagnostic hole on the drive flux on the sample surface, which includes Refs. [29–32]; for the illustration of the accurate determination of the drive flux with two independent observables; for the quantitative analysis of the difference in the implosion velocity induced by the drive flux and measured FXRD fluxes.
- [29] L. F. Jing, S. Jiang, D. Yang, H. Li, L. Zhang, Z. Lin, L. Li, L. Kuang, Y. Huang, and Y. Ding, *Phys. Plasmas* **22**, 022709 (2015).
- [30] D. H. Cohen, O. L. Landen, and J. J. MacFarlane, *Phys. Plasmas* **12**, 122703 (2005).
- [31] S. E. Jiang, Y. Huang, L. Jing, H. Li, T. Huang, and Y. Ding, *Phys. Plasmas* **23**, 012702 (2016).
- [32] L. F. Jing *et al.*, *Nucl. Fusion* **58**, 096017 (2018).
- [33] T. G. Feng, D. X. Lai, and Y. Xu, *Chin. J. Comput. Phys.* **16**, 89 (1999), <http://www.cjcp.org/CN/abstract/abstract1870.shtml>; G. L. Ren, L. Ke, Y. H. Chen, Y. S. Li, C. L. Zhai, and J. Liu, *Phys. Plasmas* **25**, 102701 (2018).
- [34] G. Mishra, K. Ghosh, A. Ray, and N. K. Gupta, *High Energy Density Phys.* **27**, 1 (2018).
- [35] C. Decker *et al.*, *Phys. Rev. Lett.* **79**, 1491 (1997).
- [36] Y. Ping *et al.*, *Nat. Phys.* **15**, 138 (2019).
- [37] T. R. Boehly, V. N. Goncharov, W. Seka, M. A. Barrios, P. M. Celliers, D. G. Hicks, G. W. Collins, S. X. Hu, J. A. Marozas, and D. D. Meyerhofer, *Phys. Rev. Lett.* **106**, 195005 (2011).
- [38] L. Y. Kuang, H. Li, L. Jing, Z. Lin, L. Zhang, L. Li, Y. Ding, S. Jiang, J. Liu, and J. Zheng, *Sci. Rep.* **6**, 34636 (2016).